On-Chip Single-Mode Distributed Feedback Colloidal Quantum Dot Laser under Nanosecond Pumping

Yunpeng Zhu,*[†,§] Weiqiang Xie,[†,§] Suzanne Bisschop,[†,‡,§] Tangi Aubert,[‡,§] Edouard Brainis,[‡,§] Pieter Geiregat,[‡,§] Zeger Hens,[‡,§] and Dries Van Thourhout[†,§]

[†]Photonics Research Group, INTEC Department, Ghent University-IMEC, Ghent B-9000, Belgium
[‡]Physics and Chemistry of Nanostructures, Ghent University, Krijgslaan 281-S3, Ghent 9000, Belgium
[§]Center of Nano and Biophotonics (NB Photonics), Ghent University, Ghent B-9000, Belgium

Ⓢ Supporting Information

ABSTRACT: We report on a hybrid integrated distributed feedback (DFB) laser fabricated using the colloidal quantum dots (QDs)/silicon nitride (SiN) integration platform. The DFB laser is fabricated with a CMOS-compatible process and consists of a waveguide stack in which a QD layer is embedded between two SiN layers to enhance the coupling of the QD to the optical waveguide mode. Following characterization of the intrinsic properties of the CdSe/CdS core/shell QDs using transient absorption spectroscopy, we demonstrate single-mode lasing upon nanosecond optical pumping. With a 7 ns pump pulse, the lasing threshold is 270 $\mu J/cm^2$. This result attests to the potential of colloidal QDs as an enabling gain material for integrated SiN photonics, and it showcases the design versatility of hybrid integrated photonics platforms based on colloidal QDs.

KEYWORDS: on-chip, single mode, colloidal quantum dots, distributed feedback laser, nanosecond pumping
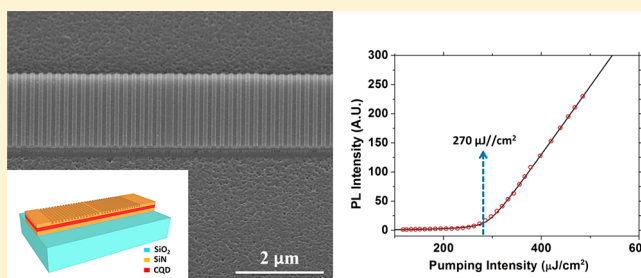
Photonic integrated circuits (PICs), originally mainly developed for telecom applications, are now finding widespread use in domains as diverse as optical interconnects, biosensing, physical sensing, spectroscopy, and quantum optics.[1−5] In this context, silicon nitride (SiN) is a particularly interesting material. The broad transparency of SiN, extending from the blue side of the visible to the near-infrared, allows addressing new wavelength domains relevant for these applications,[6] and its relatively high index (∼2.0) allows for compact PICs. Moreover, the material is very well known in the electronics industry, which enables SiN-based devices to be fabricated using cost-effective processes and opens the possibility for upscaling to large-volume and high-yield fabrication. Although the advantageous properties of SiN have been demonstrated by numerous groups,[7−12] active functionalities in general and light emission in particular are still largely missing for the SiN platform. Integrated light sources and lasers are, however, essential for building fully on-chip integrated systems, and several groups now have started integrating active materials with SiN waveguides.[13]

Colloidal quantum dots (QDs) are particularly relevant in this respect. Over the past 15 years, it has been shown that, depending on their shape, size, and composition, QDs can exhibit net optical gain at visible wavelengths.[14] Especially when synthesized as fully inorganic core/shell materials, QDs are more photostable and less prone to oxidation than other solution-processable gain media, such as organic dyes,[15] and

their emission wavelength can be readily tuned by size quantization.[14] The combination of these properties and their substrate-independent processing makes them especially promising for realizing low-cost lasers with a tunable gain spectrum.[16] Various laser devices based on colloidal QDs have been demonstrated already. However, most of these used either an accidental ad hoc resonator[17] or less versatile surface-emitting vertical cavities,[18] and some of the designs involve coated surface gratings[19,20] and silica microspheres.[21] They usually do not have a dielectric encapsulation that acts as a barrier against oxygen and moisture. In addition, these devices lack compactness, are not compatible with waveguide integration, and remain rather far from any practical implementation. Hence, an efficient integration method would considerably facilitate the use of QDs as light emitters and amplifiers in complex PICs.

As it turns out, the broad transparency window of SiN complements the wide tunability of colloidal QDs. We have therefore developed a hybrid integration platform whereby a spin-coated layer of, most often, CdSe/CdS core/shell QDs is embedded in between SiN layers[22] The integration process does not quench the QD photoluminescence and results in low-loss SiN waveguides.[22] Under femtosecond pulsed laser pumping, the embedded QDs have shown amplified sponta-

neous emission (ASE), which has been efficiently coupled to the waveguide.[23] Recently, we have demonstrated multimode disk lasers coupled to underlying bus waveguides exploiting this hybrid QD SiN integration platform,[24] to our best knowledge the first demonstration of a fully integrated QD laser. However, the fabrication process used to achieve proper light extraction is rather complex in the case of a disk laser. Moreover, such lasers are inherently multimodal, and lasing was only demonstrated upon pumping with relatively short picosecond pulses, a configuration that is not very practical in the long term.

In this paper, we demonstrate that the same SiN/QD/SiN platform can be used to form distributed feedback (DFB) lasers, in which gain is provided by an embedded QD film. This approach ensures that the QDs are fully encapsulated, and it allows to separately optimize the modal gain and the waveguiding properties of the devices. Importantly, such waveguide-coupled DFB lasers require fewer processing steps than comparable integrated disk lasers, and they are truly single mode. In addition, by incorporating CdSe/CdS QDs with suppressed Auger recombination, lasing in such integrated DFB lasers can be attained under optical pumping with a lasing threshold as low as 270 $\mu J//cm^2$ for a 7 ns pump pulse. This result underscores the design versatility that comes with using colloidal QDs as a solution-processable gain material, and it shows a way forward toward on-chip continuous wave (CW) QD lasers.

■ COLLOIDAL QUANTUM DOT PROPERTIES IN SOLUTION

To date, CdSe/CdS QDs are the most promising QDs for lasing applications, as they have shown high optical gain coefficients, long gain lifetimes, and exceptional stability[14] even after embedding into, for example, SiN. Here, we used so-called *flash* CdSe/CdS QDs, which are synthesized using a seeded growth approach that yields thick-shell CdSe/CdS QDs in a fast and simple process.[25,26] Such QDs feature an alloyed CdSe/CdS interface, which helps to reduce strain and slow down nonradiative Auger recombination of multiexcitons. The latter is important since faster Auger recombination is expected to yield higher lasing thresholds under CW operation.[27] The QDs used in this work were formed using wurtzite CdSe seed QDs with a diameter of 4 nm. The average total diameter of 11.5 nm hence corresponds to an average shell thickness of 3.75 nm. Figure 1a shows the spectrum of the intrinsic absorption coefficient for the QDs dispersed in toluene. This spectrum was determined by normalizing the QD absorbance spectrum at 350 nm to the intrinsic absorption coefficient calculated for a concentric core/shell system using the bulk optical constants of CdSe and CdS.[28] In addition, Figure 1a presents the photoluminescence spectrum of the QDs, which is centered at around 635 nm, has a line width of 29 nm, and comes with a photoluminescence quantum yield of 80%. The photoluminescence decay after nonresonant excitation is somewhat multiexponential, so we extracted an average lifetime, which amounts to 26.8 ± 0.09 ns (see inset, Figure 1a).

We assessed the potential of these QDs for optical gain by measuring the temporal nonlinear optical properties of a QD dispersion using ultrafast transient absorption (TA) spectroscopy. TA is a pump–probe technique where a sample is pumped with ultrashort laser pulses (in this case, 110 fs at a 1 kHz repetition rate) after which the change in absorbance ΔA is measured by a time-delayed probe pulse (also 110 fs) as a function of wavelength (or energy). Combining ΔA with the
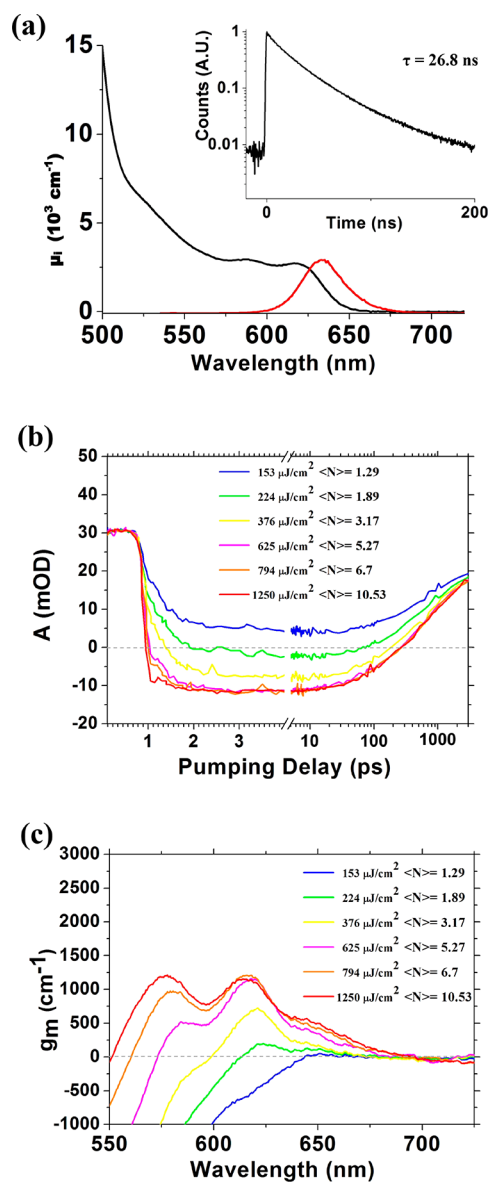
Figure 1. Overview of "flash" CdSe/CdS QDs: (a) Absorption (expressed as intrinsic absorption coefficient μ_i) and emission (red) spectrum after excitation at 400 nm. The QDs have a luminescence quantum yield of 80%. Inset: Photoluminescence (PL) decay showing an average decay time of 26.8 ± 0.09 ns. (b) Time-dependent dynamics of A at a fixed probe wavelength of 630 nm after 520 nm excitation. We can see the optical gain builds up very fast (<2 ps) and can last up to 270 ps. Importantly, from the TA traces, we estimate that the process that causes the decay of the nonlinear absorbance at the lowest fluences used has a rate constant of ~2 ns^{-1}. (c) Material gain at 2.5 ps for pumping at 520 nm. The total bandwidth can be as large as 130 nm, reaching ca. 1200 cm^{-1} at 615 nm.

linear absorption spectrum, we can obtain the absorbance A of the sample at a certain time delay and probe wavelength. If A turns negative, the dispersion exhibits optical gain, and both the gain threshold and the spectral gain window can be determined. In addition, TA spectroscopy provides the time evolution of the nonlinear absorbance, such that the rate of the processes that quench the optical gain and hence the gain or inversion lifetime can be assessed. Figure 1b represents the transient absorbance at 630 nm of the *flash* QDs dispersed in toluene, after pumping with 520 nm. The pump intensity is expressed in terms of the

average number of excitations or exciton density $\langle N \rangle$ we calculate per QD using the photon fluence and the QD absorption cross section, which is equal to 2.75×10^{-15} cm². This absorption cross section is found by multiplying the intrinsic absorption coefficient with the QD volume.[28] Overall, we observe the gain features a rapid buildup, taking less than 1 ps, even when pumping is just above threshold. The gain features can last up to 270 ps for the highest pump fluence used. Importantly, from the TA traces, we estimate that the process that causes the decay of the nonlinear absorbance at the lowest fluences used has a rate constant of ~ 2 ns^{-1}. Such a figure is reasonable for a gain process dominated by Auger recombination of biexcitons in these CdSe/CdS core/shell QDs.[29]

Importantly, since the (nonlinear) absorbance is a quantity that depends on the QD concentration, we prefer to express the TA data for further analysis in terms of the material gain, which is obtained by normalizing the nonlinear absorbance using the intrinsic absorption coefficient at a reference wavelength λ_{ref} (taken here as 350 nm):

$$g_m(\lambda, t) = -A(\lambda, t) \frac{\mu_{i,0}(\lambda_{ref})}{A_0(\lambda_{ref})} \qquad (1)$$

Figure 1c plots the thus calculated material gain spectrum at a 2.5 ps time delay for different pump fluences. It can be seen from the results that gain is first attained at the long-wavelength side (>640 nm) of the band-edge absorption feature, when increasing the exciton density beyond 1.2 exciton per QD ($\langle N_{av} \rangle = 1.2$), in line with theoretical predictions.[26] Increasing the pump fluence broadens the gain spectrum and enhances the material gain. Eventually, the gain window extends from 550 to 680 nm, and the material gain levels off at maximum values of around 1200 cm^{-1} at 615 nm.

■ COLLOIDAL QUANTUM DOT EMBEDDED IN A WAVEGUIDE

Figure 2 shows the proposed hybrid SiN-QD DFB laser and the associated fabrication flow. The *flash* QDs described in the previous section are embedded between two layers of SiN to enhance the coupling betwe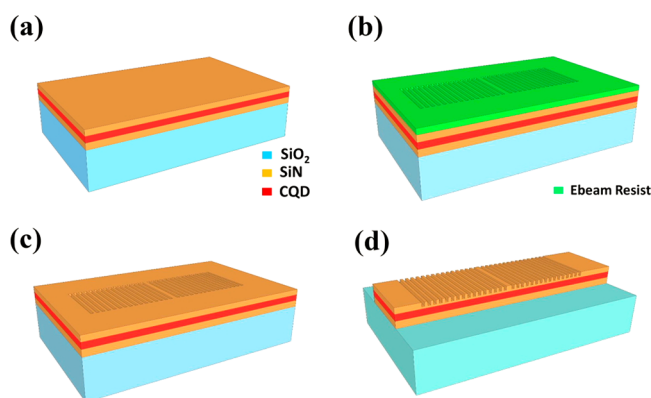en the QD emission and the optical mode of the waveguide. Starting from a silicon wafer with a 3 μm thermal oxide grown on top, a first SiN layer is deposited. The deposition is performed using an optimized plasma-enhanced chemical vapor deposition (PECVD) process at a temperature of 270 °C. Next, *flash* QDs are spin coated on top of this SiN layer to form a densely packed layer with a thickness of approximately 50 nm, as measured with a Dektak surface profiler. Another SiN layer is then deposited, again at a temperature of 270 °C. This encapsulates the QD layer and completes the SiN/QD/SiN sandwich stack. Next, electron-beam (e-beam) lithography is used to define the DFB grating, as shown by Figure 2b. Through CF$_4$/H$_2$ reactive ion etching (RIE), the grating pattern is transferred to the top SiN layer (Figure 2c), after which the residual resist is stripped using an oxygen plasma. Finally, the waveguide ridge is defined using standard contact lithography and a second RIE process (Figure 2d).

In a first experiment, we used a waveguide-based variable stripe length method to determine the modal gain of waveguides defined in the SiN/QD/SiN stack.[23] Instead of using a slit with variable width to control the extent of the pumping spot, we use an array of waveguides with gradually increasing length. The waveguides are formed in a 100 nm/50 nm/100 nm SiN/QD/SiN stack using the process described in Figure 2, but leaving out the e-beam step. Figure 3a shows the scanning electron microscope (SEM) picture of the cross section of the fabricated waveguide with details of the layer stack inserted. The waveguides vary in length, from 40 to 600 μm with a fixed step of 10 μm. The chip was cleaved after the

Figure 2. Fabrication overview. (a) First, a SiN layer is deposited on a silicon substrate with a 3 μm thermal silicon oxide grown on top. Next, the QD layer is spin coated on top, and another SiN layer is deposited on the QD layer to encapsulate the QDs and form the hybrid SiN/QD/SiN stack. (b) Electron beam lithography to pattern the grating. (c) RIE etching to transfer the grating patterning to the top SiN layer. (d) Contact lithography and RIE etching to pattern the waveguide.
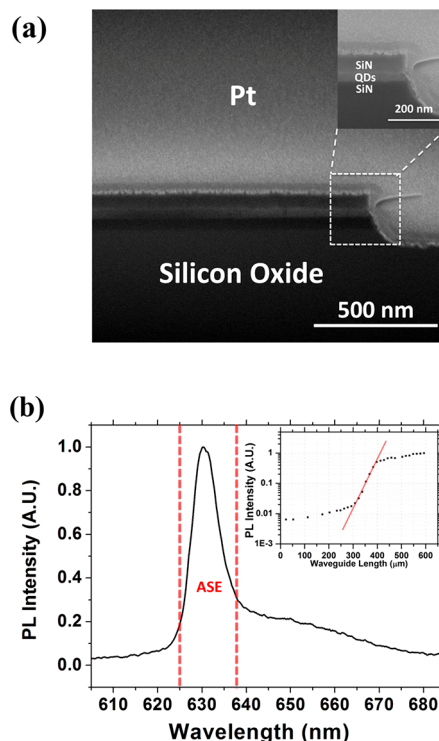
Figure 3. QD properties in the waveguide. (a) Scanning electron microscope (SEM) picture of the fabricated waveguide cross section. The details are inset. (b) Emission spectrum of a 600 μm long waveguide with a pumping fluence 54 μJ/cm² @ 400 nm. Inset: Waveguide gain measurement results: ASE intensity (in log scale) versus the waveguide length (black dotted) with fit of the exponential intensity increase (red solid line).

C

lithography step but before the RIE process to ensure a uniform facet. The etching process was optimized to ensure a smooth sidewall.[22] As demonstrated in previous work, such waveguides with embedded QDs feature a propagation loss of only a few dB/cm.[22]

The waveguide modal gain was then characterized using a femtosecond laser system (see Supporting Information S1). The 110 fs pulses at a 1 kHz repetition rate and a wavelength of 800 nm are frequency doubled in a beta barium borate (BBO) crystal. The resulting 400 nm pulses are used to pump the waveguide array using a cylindrical lens, which focuses the laser beam into a strip measuring ~8 by 0.04 mm. The focused beam is adjusted to overlap with the waveguides, and the light emitted from the waveguide facet is collected by a multimode fiber (NA = 0.2). Neutral density (ND) filters are used to tune the pump power. Figure 3b shows the collected spectrum from a 600 μm long waveguide pumped at a fluence of 54 μJ/cm^2 @ 400 nm. The spectrum is approximately centered at 632 nm and exhibits a full width at half-maximum (fwhm) of 6.5 nm. This is clearly narrowed down compared to the low fluence spontaneous emission (SE) spectrum, indicative of amplified spontaneous emission. The ASE peak develops at the high-energy side of the spontaneous PL peak. The inset picture of Figure 3b shows the measured output power versus the waveguide length, at a constant pump fluence of 56 μJ/cm^2. The figure shows a pronounced superlinear rise in emission intensity for waveguides longer than ~280 μm, and the emission saturates for waveguides with lengths exceeding ~400 μm. We estimate the net modal gain g by fitting the length-dependent intensity within the region of exponential intensity increase to the function

$$I = A_0 \left[\frac{e^{gL} - 1}{g} + \frac{R}{g} e^{2gL} (1 - e^{-gL}) \right] \tag{2}$$

whereby R is the reflection of the back facet of the waveguides (see Supporting Information S2). For R varying from 0 to 5%, the fit yields a net modal gain of around 350−212 cm^{-1}.

DFB GRATING DESIGN AND FABRICATION

The DFB lasers were fabricated starting from a 75 nm/50 nm/90 nm SiN/QD/SiN sandwich layer. First-order gratings were defined with a $\lambda/4$ phase shift section inserted in the middle to form the laser cavity. To optimize the grating parameters (etch depth, period), 3D finite-difference time-domain (FDTD) simulations were carried out, from which we determined the grating Bragg wavelength and stopband. The indexes of the SiN layer and the QD layer were measured using ellipsometry and found to be $n_{SiN} = 2.0$ and $n_{QD} = 1.9$. The grating etching depth was fixed to 35 nm, and a 50% duty cycle was assumed. The waveguide width was set at 2 μm. Figure 4a shows the calculated grating band gap versus period. The gray and red regions denote the upper and lower stopband areas, respectively. The simulated photonic band gap is around 14 nm. Clearly, we should carefully choose the grating period to ensure that the photonic band gap overlaps with the measured QD ASE spectrum. To take into account uncertainties in the fabrication process, we therefore fabricated DFB lasers with a grating period varying from 180 to 195 nm on the same chip. Figure 4b shows a cross section taken in the phase shifter area. In this case, the grating period is 188 nm and the etch depth is around 35 nm, the value targeted for during the design. At the back-side the lasers are connected to a waveguide without
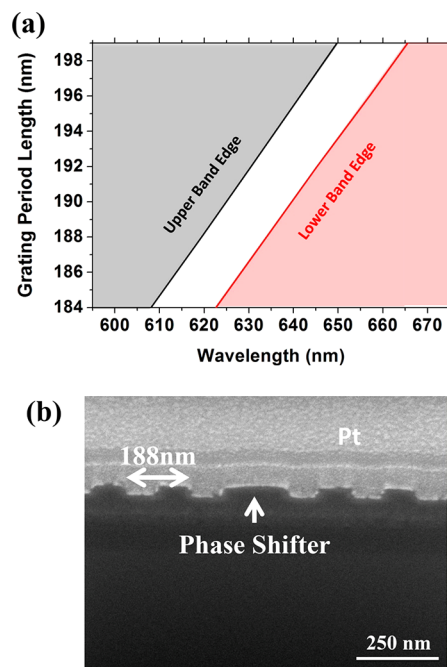
(a)

(b)

Figure 4. Design of the DFB grating and fabricated samples. (a) The waveguide stack, from bottom to top, consists of 3 μm SiO$_2$, 75 nm SiN, 50 nm QDs layer, 90 nm SiN (with a 35 nm grating etching depth) and a filling factor of 0.5. The simulated stopband of the grating has been shown in the picture as the region between the gray and red areas. (b) Cross section of the fabricated DFB laser in the $\lambda/4$ phase shifter region. The etching depth is 35 nm as designed.

grating, which ensures low residual reflections. The laser cavity length is approximately 100 μm.

LASER CHARACTERIZATION

We first characterize the DFB lasers' properties using the femtosecond laser setup described above. The emission from the waveguide facet was collected by a multimode fiber for analysis. The light(in)−light(out) curve (see Supporting Information S3) shows a clear threshold around 12 μJ/cm^2 (@ 400 nm), a first indication that the device is lasing. Figure 5a shows the emission spectra of three devices with varying grating period (pumping fluence = 15 μJ/cm^2 @ 400 nm). The ASE spectrum taken from a waveguide without grating is overlaid on top for comparison. The measured spectra show the lasers are operating in a single longitudinal mode, with a high side mode suppression ratio. The three lasers exhibit a 1 nm difference in grating period, which results in a 2.6 nm shift in the measured spectra, in line with simulations (dλ/dΛ = 2.64). The lasing peaks have a 0.2 nm fwhm and fall within the ASE envelope.

To further investigate the laser performance, we used a Q-switched frequency-doubled Nd:YAG laser (532 nm) with a 7 ns pulse width and a 938 Hz repetition rate for pumping. Again, the laser light was focused with a cylindrical lens to a rectangular pattern to pump the DFB, this time measuring ~3.15 by 0.07 mm^2 (see Supporting Information S4). Figure 5b and c show the power emitted from the cleaved facet measured as a function of pump fluence, respectively, on a double-linear (Figure 5b) and a double-logarithmic (Figure 5c) scale. The linearly scaled graph shows a clear lasing threshold at 270 μJ/cm^2. Taking into account the pulse length (7 ns), the equivalent CW pump fluence (power per pulse divided by the pulse time

(a)

(b)

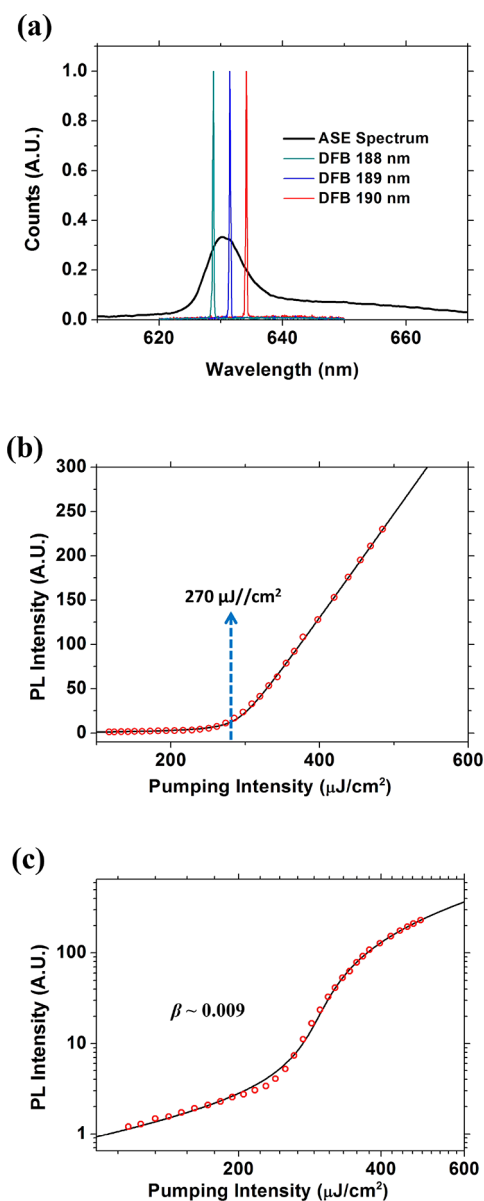270 μJ//cm²

(c)

β ~ 0.009

Figure 5. Laser characterization. (a) Spectra measured from an unpatterned waveguide (black) and DFB lasers with different grating periods (colored). (b) The light(in)−light(out) curve on a double linear scale, with indication of the lasing threshold around 270 μJ/cm², which has an equivalent CW power density of 39 kW/cm². (c) Light(in)−light(out) curve on a double log-scale with rate equation fit (black solid). A spontaneous emission factor (β) of 0.009 is extracted.

width) is then 39 kW/cm². The experimental data of Figure 5c was fitted to a static rate equation model (see Supporting Information S5), from which a spontaneous emission factor (β) of 0.009 was extracted.

The DFB laser's κL, where κ is the coupling coefficient and L is the length of the DFB cavity, is a measure of the strength of the grating and was calculated to be 16.7 using the equation[30]

$$\kappa L = \sqrt{\left(\frac{\Delta\lambda\pi n_{\text{eff}}L}{\lambda_{\text{Bragg}}^2}\right)^2 - \pi^2} \tag{3}$$

In this equation, $\Delta\lambda$ is the stopband width, which can be deduced from the spontaneous emission spectrum with and without grating (see Supporting Information S6). λ_{Bragg} is the

grating Bragg wavelength, and n_{eff} is the effective index of the waveguide. The large κL indicates our DFB grating provides strong feedback, contributing to the laser's low threshold fluence.[31] It also means that the cavity photon lifetime is given by[30]

$$\frac{1}{\tau_{\text{ph}}} = [\alpha_{\text{int}} + 4\kappa\,e^{(-\kappa L)}]v_{\text{g}} \tag{4}$$

where v_{g} is the group velocity. The above equation indicates the cavity photon lifetime is dominated by the internal losses a_{int}. These could include waveguide scattering losses but also losses due to photon induced intraband transitions. We can estimate a_{int} to be on the order of 2.5−20 cm^{-1}, equivalent to a photon lifetime of 30−3 ps. Compared to the 2 ns^{-1} decay rate, our 7 ns pump actually can be considered as quasi-CW. This observation allows using the model developed by Park et al.[27] to analyze and predict the CW pumping threshold of our device. This model links the average QD occupancy $\langle N^* \rangle$ to the pump fluence J as

$$\langle N^* \rangle = \frac{J\sigma\tau_x + 2(J\sigma)^2\tau_x\tau_{xx}}{1 + J\sigma\tau_x + (J\sigma)^2\tau_x\tau_{xx}} \tag{5}$$

where τ_x and τ_{xx} are the single exciton and biexciton lifetimes and σ is the absorption cross section. For the QDs used, the single exciton lifetime is 26.8 ns, as was derived from Figure 1b. From the gain decay rate we estimate the biexciton lifetime to be ~500 ps. The absorption cross section is 2.75×10^{-15} cm², as mentioned in the previous section. By using this data, and assuming a 30 ps cavity photon lifetime, we can estimate a minimum lasing threshold intensity around 10.9 kW/cm². If the cavity photon lifetime reduces to 3 ps, the theoretical lasing threshold intensity increases to 46.2 kW/cm². If we take into account that a fraction of the incident pump gets reflected by the layer interfaces, our observed equivalent CW pump intensity of 39 kW/cm² falls right within this range.

■ DISCUSSION AND CONCLUSION

Previous reports showed colloidal QD lasers operating under nanosecond,[32−34] microsecond excitations.[35] Recently, CW-pumped lasing has been demonstrated with colloidal QDs coating photonic crystal DFBs.[16] Our work extends these results by demonstrating a truly integrated QD laser operating under nanosecond pulsed excitation. This is altogether a remarkable feat, as the 2 ns^{-1} decay rate for the gain makes 7 ns pumping almost equivalent to quasi-CW operation. Theoretical modeling built from previous work[27] agrees well with our experimental results. There are several aspects that allow our DFB lasers to exhibit a low lasing threshold and to operate in a quasi-CW pumping regime. Most importantly, the *flash* quantum dots we are using have a suppressed nonradiative Auger recombination rate, which is now well understood to be essential for lasing applications.[14,27] Moreover, our optimized embedding process not only preserves the emission properties of the QDs but also enhances the coupling between the QD emission and the optical mode of the cavity. In this way, by combining the QDs with a SiN PIC platform, on-chip optical microcavities with compact size and low optical loss are achieved.

Using QDs with further increased biexciton lifetime could still substantially reduce the lasing threshold. Also some other techniques might further improve the QD laser performance. Using inorganic-halide-capped QDs etc.[35] could increase the

packing density in the active layer, resulting in a higher modal gain and better thermal conductivity. Alternatively a ZnS shell could be used to cap the current QDs and better preserve their optical properties after encapsulation into the SiN layer stack. It may also be relevant to provide on-chip heat sinking structures to avoid local heating that quenches the QD emission.

Even without these possible improvements, the laser equivalent CW threshold that we currently observe is at the same level as that of III−V semiconductor lasers epitaxially grown on silicon.[36] This opens strong prospects in terms of CW operation and, consequently, an extended application potential. One could now realistically envision CW-pumped on-chip integrated lasers using colloidal quantum dots as the gain medium. The intrinsic combination with the mature SiN waveguide platform then immediately opens the path toward more complex devices such as tunable lasers and arrays of single-mode lasers or integration with passive structures such as on-chip spectrometers. This in turn will enable applications such as on-chip biosensing, absorption spectroscopy, and Raman spectroscopy, which now require off-chip sources and complex optical coupling approaches.[37,38]

In conclusion, we have reported the design and fabrication of on-chip single-mode DFB lasers based on a hybrid QD-SiN platform. We reported for the first time single-mode lasing under nanosecond pulsed excitation at 532 nm for colloidal QD based integrated lasers. The lasing threshold of the DFB device is as low as 270 μJ/cm^2, using 7 ns long pulses, opening up the road toward realizing CW-pumped on-chip integrated devices.

◼ ASSOCIATED CONTENT

ⓢ Supporting Information

The Supporting Information is available free of charge on the ACS Publications website at DOI: 10.1021/acsphotonics.7b00644.

> Measurement setup, waveguide-based variable stripe length method with reflection, light (in)−light (out) measurement with femtosecond laser, pump laser beam calibration, rate equation analysis of L−L curves, stopband measurement of the DFB laser grating, PL decay time in SiN layer stack (PDF)

◼ AUTHOR INFORMATION

Corresponding Author

*E-mail: yunpeng.zhu@ugent.be.

ORCID Ⓞ

Yunpeng Zhu: 0000-0002-5200-6581
Edouard Brainis: 0000-0003-4720-1793
Zeger Hens: 0000-0002-7041-3375

Author Contributions

D.v.T., Z.H., and E.B. directed the research. Y.Z. performed the design, fabrication, and characterization of the DFB laser. S.B. performed the TAS measurement. T.A. provided the QDs. W.X. and P.G. helped with results analysis and the data fitting. All authors discussed the results and contributed to the manuscript.

◼ REFERENCES

(1) Miller, D. A. Optical interconnects to silicon. *IEEE J. Sel. Top. Quantum Electron.* **2000**, *6* (6), 1312−7.

(2) Lai, W. C.; Chakravarty, S.; Zou, Y.; Chen, R. T. Silicon nano-membrane based photonic crystal microcavities for high sensitivity bio-sensing. *Opt. Lett.* **2012**, *37* (7), 1208−10.

(3) Liu, Y.; Salemink, H. W. Photonic crystal-based all-optical on-chip sensor. *Opt. Express* **2012**, *20* (18), 19912−20.

(4) Redding, B.; Liew, S. F.; Sarma, R.; Cao, H. Compact spectrometer based on a disordered photonic chip. *Nat. Photonics* **2013**, *7* (9), 746−51.

(5) Politi, A.; Cryan, M. J.; Rarity, J. G.; Yu, S.; O'brien, J. L. Silica-on-silicon waveguide quantum circuits. *Science* **2008**, *320* (5876), 646−9.

(6) Subramanian, A. Z.; Ryckeboer, E.; Dhakal, A.; Peyskens, F.; Malik, A.; Kuyken, B.; Zhao, H.; Pathak, S.; Ruocco, A.; De Groote, A.; Wuytens, P. Silicon and silicon nitride photonic circuits for spectroscopic sensing on-a-chip [Invited]. *Photonics Res.* **2015**, *3* (5), B47−59.

(7) Stutius, W.; Streifer, W. Silicon nitride films on silicon for optical waveguides. *Appl. Opt.* **1977**, *16* (12), 3218−22.

(8) Hosseini, E. S.; Yegnanarayanan, S.; Atabaki, A. H.; Soltani, M.; Adibi, A. High Quality Planar Silicon Nitride Microdisk Resonators for Integrated Photonics in the VisibleWavelength Range. *Opt. Express* **2009**, *17* (17), 14543−51.

(9) Ghulinyan, M.; Guider, R.; Pucker, G.; Pavesi, L. Monolithic whispering-gallery mode resonators with vertically coupled integrated bus waveguides. *IEEE Photonics Technol. Lett.* **2011**, *23* (16), 1166−8.

(10) Subramanian, A. Z.; Neutens, P.; Dhakal, A.; Jansen, R.; Claes, T.; Rottenberg, X.; Peyskens, F.; Selvaraja, S.; Helin, P.; Du Bois, B.; Leyssens, K. Low-loss singlemode PECVD silicon nitride photonic wire waveguides for 532−900 nm wavelength window fabricated within a CMOS pilot line. *IEEE Photonics J.* **2013**, *5* (6), 2202809.

(11) Bauters, J. F.; Heck, M. J.; John, D.; Dai, D.; Tien, M. C.; Barton, J. S.; Leinse, A.; Heideman, R. G.; Blumenthal, D. J.; Bowers, J. E. Ultra-low-loss high-aspect-ratio Si 3 N 4 waveguides. *Opt. Express* **2011**, *19* (4), 3163−74.

(12) Dai, D.; Wang, Z.; Bauters, J. F.; Tien, M. C.; Heck, M. J.; Blumenthal, D. J.; Bowers, J. E. Low-loss Si 3 N 4 arrayed-waveguide grating (de) multiplexer using nano-core optical waveguides. *Opt. Express* **2011**, *19* (15), 14130−6.

(13) Zhao, H.; Kuyken, B.; Clemmen, S.; Leo, F.; Subramanian, A.; Dhakal, A.; Helin, P.; Severi, S.; Brainis, E.; Roelkens, G.; Baets, R. Visible-to-near-infrared octave spanning supercontinuum generation in a silicon nitride waveguide. *Opt. Lett.* **2015**, *40* (10), 2177−80.

(14) Pietryga, J. M.; Park, Y. S.; Lim, J.; Fidler, A. F.; Bae, W. K.; Brovelli, S.; Klimov, V. I. Spectroscopic and Device Aspects of Nanocrystal Quantum Dots. *Chem. Rev.* **2016**, *116* (18), 10513−622.

(15) Burrows, P. E.; Shen, Z.; Bulovic, V.; McCarty, D. M.; Forrest, S. R.; Cronin, J. A.; Thompson, M. E. Relationship between electro-luminescence and current transport in organic heterojunction light - emitting devices. *J. Appl. Phys.* **1996**, *79* (10), 7991−8006.

(16) Fan, F.; Voznyy, O.; Sabatini, R. P.; Bicanic, K. T.; Adachi, M. M.; McBride, J. R.; Reid, K. R.; Park, Y. S.; Li, X.; Jain, A.; Quintero-Bermudez, R. Continuous-wave lasing in colloidal quantum dot solids enabled by facet-selective epitaxy. *Nature* **2017**, *544*, 7510.1038/nature21424.

(17) Wang, Y.; Ta, V. D.; Gao, Y.; He, T. C.; Chen, R.; Mutlugun, E.; Demir, H. V.; Sun, H. D. Stimulated emission and lasing from CdSe/CdS/ZnS core - multi - shell quantum dots by simultaneous three - photon absorption. *Adv. Mater.* **2014**, *26* (18), 2954−61.

(18) Dang, C.; Lee, J.; Breen, C.; Steckel, J. S.; Coe-Sullivan, S.; Nurmikko, A. Red, green and blue lasing enabled by single-exciton gain in colloidal quantum dot films. *Nat. Nanotechnol.* **2012**, *7* (5), 335−9.

(19) Roh, K.; Dang, C.; Lee, J.; Chen, S.; Steckel, J. S.; Coe-Sullivan, S.; Nurmikko, A. Surface-emitting red, green, and blue colloidal quantum dot distributed feedback lasers. *Opt. Express* **2014**, *22* (15), 18800−6.

(20) Dang, C.; Lee, J.; Roh, K.; Kim, H.; Ahn, S.; Jeon, H.; Breen, C.; Steckel, J. S.; Coe-Sullivan, S.; Nurmikko, A. Highly efficient, spatially coherent distributed feedback lasers from dense colloidal quantum dot films. *Appl. Phys. Lett.* **2013**, *103* (17), 171104.

(21) Min, B.; Kim, S.; Okamoto, K.; Yang, L.; Scherer, A.; Atwater, H.; Vahala, K. Ultralow threshold on-chip microcavity nanocrystal quantum dot lasers. *Appl. Phys. Lett.* **2006**, *89* (19), 191124.

(22) Xie, W.; Zhu, Y.; Aubert, T.; Verstuyft, S.; Hens, Z.; Van Thourhout, D. Low-loss silicon nitride waveguide hybridly integrated with colloidal quantum dots. *Opt. Express* **2015**, *23* (9), 12152−60.

(23) Zhu, Y, Xie, W, Geiregat, P, Bisschop, S, Aubert, T, Brainis, E, Hens, Z, Thourhout, D. V. Hybrid colloidal quantum dot silicon nitride waveguide gain measurement based on variable stripe length method. *InCLEO: Applications and Technology*; Optical Society of America, 2016; pp ATh1J-5.

(24) Xie, W., Stöferle, T., Rainò, G., Aubert, T., Bisschop, S., Zhu, Y., Mahrt, R. F., Geiregat, P., Brainis, E., Hens, Z., Van Thourhout, D. On - Chip Integrated Quantum - Dot−Silicon - Nitride Microdisk Lasers. *Adv. Mater.* **2017**, *29* (16), 160486610.1002/adma.201604866.

(25) Cirillo, M.; Aubert, T.; Gomes, R.; Van Deun, R.; Emplit, P.; Biermann, A.; Lange, H.; Thomsen, C.; Brainis, E.; Hens, Z. "Flash" Synthesis of CdSe/CdS Core−Shell Quantum Dots. *Chem. Mater.* **2014**, *26* (2), 1154−60.

(26) Drijvers, E.; De Roo, J.; Geiregat, P.; Fehér, K.; Hens, Z.; Aubert, T. Revisited Wurtzite CdSe Synthesis: A Gateway for the Versatile Flash Synthesis of Multishell Quantum Dots and Rods. *Chem. Mater.* **2016**, *28* (20), 7311−23.

(27) Park, Y. S.; Bae, W. K.; Baker, T.; Lim, J.; Klimov, V. I. Effect of Auger recombination on lasing in heterostructured quantum dots with engineered core/shell interfaces. *Nano Lett.* **2015**, *15* (11), 7319−28.

(28) Hens, Z.; Moreels, I. Light absorption by colloidal semiconductor quantum dots. *J. Mater. Chem.* **2012**, *22* (21), 10406−15.

(29) Bae, W. K.; Padilha, L. A.; Park, Y. S.; McDaniel, H.; Robel, I.; Pietryga, J. M.; Klimov, V. I. Controlled alloying of the core−shell interface in CdSe/CdS quantum dots for suppression of Auger recombination. *ACS Nano* **2013**, *7* (4), 3411−9.

(30) Geert, M.; Vankwikelberge, P. *Handbook of Distributed Feedback Laser Diodes*; Artech House, 2013.

(31) Whiteaway, J. E.; Thompson, G. H.; Collar, A. J.; Armistead, C. J. The design assessment of lambda/4 phase-shifted DFB laser structures. *IEEE J. Quantum Electron.* **1989**, *25* (6), 1261−79.

(32) Guilhabert, B.; Foucher, C.; Haughey, A. M.; Mutlugun, E.; Gao, Y.; Herrnsdorf, J.; Sun, H. D.; Demir, H. V.; Dawson, M. D.; Laurand, N. Nanosecond colloidal quantum dot lasers for sensing. *Opt. Express* **2014**, *22* (6), 7308−19.

(33) McLellan, L. J.; Guilhabert, B.; Laurand, N.; Dawson, M. D. CdS x Se 1-x/ZnS semiconductor nanocrystal laser with sub 10kW/cm 2 threshold and 40nJ emission output at 600 nm. *Opt. Express* **2016**, *24* (2), A146−53.

(34) Yakunin, S.; Protesescu, L.; Krieg, F.; Bodnarchuk, M. I.; Nedelcu, G.; Humer, M.; De Luca, G.; Fiebig, M.; Heiss, W.; Kovalenko, M. V. Low-threshold amplified spontaneous emission and lasing from colloidal nanocrystals of caesium lead halide perovskites. *Nat. Commun.* **2015**, *6*, 8056.

(35) Adachi, M. M., Fan, F., Sellan, D. P., Hoogland, S., Voznyy, O., Houtepen, A. J., Parrish, K. D., Kanjanaboos, P., Malen, J. A., Sargent, E. H. Microsecond-sustained lasing from colloidal quantum dot solids. *Nat. Commun..* **2015**, *6*, 869410.1038/ncomms9694.

(36) Wang, Z.; Tian, B.; Pantouvaki, M.; Guo, W.; Absil, P.; Van Campenhout, J.; Merckling, C.; Van Thourhout, D. Room-temperature InP distributed feedback laser array directly grown on silicon. *Nat. Photonics* **2015**, *9* (12), 837−42.

(37) Martens, D., Bienstman, P. Comparison between Vernier-cascade and MZI as transducer for biosensing with on-chip spectral filter. *Nanophotonics* **2017**.10.1515/nanoph-2016-0181

(38) Dhakal, A.; Wuytens, P. C.; Peyskens, F.; Jans, K.; Thomas, N. L.; Baets, R. Nanophotonic waveguide enhanced Raman spectroscopy of biological submonolayers. *ACS Photonics* **2016**, *3* (11), 2141.